Thermal decomposition characterization of supergene potassium-jarosite and sodium-jarosite minerals from the northern Tibetan Plateau, China

Lei Chen

MLR Key Laboratory of Metallogeny and Mineral Assessment, Institute of Mineral Resources, Chinese Academy of Geological Sciences, Beijing 100037, China

Corresponding author: chenlei1211@cags.ac.cn (Lei Chen)

Abstract: The thermal decomposition of supergene potassium-jarosite and sodium-jarosite samples from the weathering profiles of sulfide deposits in the northern Tibetan Plateau, China, was investigated. Electron microprobe, scanning electron microscopy, and X-ray diffraction analyses indicated the presence of nearly pure potassium-jarosite and sodium-jarosite. Thermogravimetric analysis of the potassium-jarosite sample revealed mass losses of 11.39 wt% at 443.0 °C, 20.99 wt% at 688.3 °C, and 3.18 wt% at 779.3 °C. The thermogravimetric analysis of sodium-jarosite revealed mass losses of 11.72 wt% at 447.5 °C, 21.32 wt% at 682.6 °C, and 3.70 wt% at 716.5 °C. The results provide no evidence for water-molecule loss below 400 °C, as has been reported previously for natural potassium-jarosite and sodium-jarosite. Thermal-decomposition mechanisms have been proposed for potassium-jarosite and sodium-jarosite based on X-ray diffraction analyses of samples obtained at distinct points along the respective thermal decomposition processes. A comparison of the thermal analysis patterns of potassium-jarosite and sodium-jarosite indicates that sodium-jarosite undergoes the initiation of lattice destruction at a higher temperature.

Keywords: potassium-jarosite, sodium-jarosite, thermogravimetric analysis, X-ray diffraction

1. Introduction

Jarosite is a subgroup mineral of the alunite supergroup that has the generalized composition $AB_3(XO_4)_2(OH)_6$, where A = Na^+, K^+, Ag^+, Rb^+, H_3O^+, NH^{4+}, Pb^{2+}, B = Fe^{3+}, Al^{3+}, Cr^{3+}, and X = S or, less commonly, As or P (Scott, 1987; Jambor, 1999; Dutrizac and Jambor, 2000; Stoffregen et al., 2000). Jarosite minerals have a trigonal crystal structure in the space group R-3m, and are characterized by B = Fe^{3+} and X = S. Potassium-jarosite $[KFe_3(SO_4)_2(OH)_6]$ and sodium-jarosite $[NaFe_3(SO_4)_2(OH)_6]$ are common components. Supergene jarosite minerals are frequently observed in sulfate-rich environments formed from sulfide sediments, acid mine drainage, and weathering profiles derived from pyrite-bearing ore deposits, and are formed under highly acidic and oxidizing conditions (Rye and Alpers, 1997).

The thermal decomposition of jarosite minerals has been investigated for some time using thermogravimetric analysis (TGA) and differential thermal analysis (DTA), and various thermal-decomposition mechanisms have been proposed. Kulp and Adler (1950) showed that the decomposition of jarosite minerals occurred in two distinct steps: dehydroxylation at ~400 °C via the loss of H_2O; and desulfonation at ~700 °C via the loss of SO_3. Further studies demonstrated that jarosite minerals underwent five distinct decomposition steps: dehydration (190–340 °C), deprotonation (240–440 °C), minor dehydroxylation (300–510 °C), primary dehydroxylation (540 °C), and desulfonation (560–930 °C) (Kubisz, 1971). Frost et al. (2005) argued that jarosite loses its hydroxyl units at ~220 °C. This finding is in contrast with other results that indicate that the first decomposition step is the loss of H_3O^+ from the crystal structure, and that dehydroxylation and desulfonation occur

in two distinct steps (Alpers and Brimhall, 1989; Drouet and Navrotsky, 2003). Natural jarosite minerals can form over a wide range of physicochemical conditions (Rye and Alpers, 1997; Rye et al., 2000), however, the end-member jarosite minerals are difficult to segregate physically because of various substitutions of cations in different crystallographic sites. As a result, previous studies have used synthetic jarosite materials as analogs for natural jarosite to determine thermal-decomposition mechanisms. In general, however, synthesis conditions in the laboratory differ substantially from those in nature, which can lead to variations in structure. For example, some synthetic jarosite materials appear to include site vacancies, iron deficiencies, or significant H_3O^+ substitutions in the crystal structure that are not observed in natural supergene jarosite minerals (Desborough et al., 2010). Thus, the study of natural jarosite minerals may provide valuable information regarding thermal-decomposition mechanisms. Despite previous research studies on natural jarosite minerals, their compositions were not presented and it is not clear exactly which jarosite minerals were studied.

In this study, we present a detailed comparison of mineralogical, chemical, and thermal analyses of supergene potassium-jarosite and sodium-jarosite minerals obtained from the weathering profiles of sulfide deposits in the northern Tibetan Plateau, China. In addition, we examine the influence of substitutions on the decomposition temperatures. Complementary techniques, including X-ray diffraction (XRD), scanning electron microscopy (SEM), electron microprobe (EMP), and thermogravimetric /differential thermal analysis (TGA/DTA) were used to characterize these minerals. The results provide a better understanding of the decomposition mechanisms of both natural supergene potassium-jarosite and sodium-jarosite.

2. Materials and Methods

2.1 Samples

We chose two representative end-member K- and Na-jarosite minerals from two massive sulfide ore deposits in northern margin of Tibetan Plateau (Chen, 2012). A sample of supergene potassium-jarosite (denoted BY06-35) with banded textures was collected from the weathering profiles in the Baiyin VHMS Fe-Cu deposit (36°40′–36°36′N, 104°11′–104°19′E), northwestern China. A sample of sodium-jarosite (denoted XTS15) with botryoidal textures was collected from the weathering profiles in the Xitieshan Pb-Zn deposit (37°19′55″N, 95°34′48″E), northwestern China. The textural characteristics of the samples indicate that potassium-jarosite and sodium-jarosite were precipitated directly from the weathering solutions (Chen et al., 2013; Chen and Li, 2014). The environmental parameters of potassium-jarosite and sodium-jarosite precipitated are shown in Table 1. Polished thin sections of each specimen were examined under an optical microscope to determine the purity of the samples and the number of phases represented. After petrographic examination, suitable portions of each sample were crushed, washed in distilled water in an ultrasonic bath for 40–50 min, and allowed to dry undisturbed in air. For each sample, 30–50 grains of visually pure jarosite minerals, ranging from 1 to 2 mm in diameter, were handpicked under a binocular microscope. The purity, composition, and crystallinity of these grains were investigated by a combination of XRD, SEM, and EMP analysis at the State Key Laboratory of Geological Processes and Mineral Resources, China University of Geosciences (Wuhan).

Table 1. The comparison of potassium-jarosite and sodium-jarosite precipitated environmental parameters

Sample	Formation temperature	zonation	age	Parent rock
BY06-35	6~9°C (Chen 2012)	No	4.36±0.12 Ma (Chen 2012)	Fe-Cu sulfide ore
XTS15	5.3°C (Chen et al., 2013)	No	2.2~0.1 Ma (Chen 2012)	Pb-Zn sulfide ore

2.2 X-ray diffraction

Powder XRD patterns were collected with an X'Pert PRO DY2198 operated at 40 kV and 30 mA using Cu-Kα radiation (λ = 1.54056 Å) with a 2θ scan speed of 2°/min. The unit cell parameters of the

minerals were calculated by least-squares refinement methods using JADE 9.0 software (Materials Data Inc., Livermore, California, U.S.A.).

2.3 Scanning electron microscopy and electron microprobe analysis

SEM characterization was conducted using an FEI Quanta 200 instrument that allowed for the combined analysis of sample morphology and texture. The chemical compositions of the minerals were determined using a JEOL JXA-8900 fully automated five-spectrometer microprobe operated at a 15 kV accelerating voltage and a 10 nA (cup) current. The electron beam was defocused to a 5 μm diameter to reduce Na and K migration. Analytical uncertainties for major and minor elements were approximately ± 2% (1σ) and approximately ± 3% for trace elements based on counting statistics. Orthoclase, albite, PbF_2, hematite, anorthite, barite, apatite and InAs were used as standards for K (190 ppm), Na (190 ppm), Pb (980 ppm), Fe (920 ppm), Al (110 ppm), S (260 ppm), P (220 ppm), and As (370 ppm), respectively. Detection limits were calculated at the 3σ level. For the EMP data, the concentration (mol%) of K, Na, and Fe in *A* and *B* sites were normalized to two S atoms per chemical formula based on the ideal jarosite mineral formula in which the sulfate tetrahedron is fully occupied by S. The concentration of H_2O was calculated by difference assuming that all jarosite components sum to 100% by weight.

2.4 Thermogravimetric analysis

TGA presents the mass loss as a function of temperature (TGA curve), and the first derivative of the TGA curve shows the temperature at which mass loss occurs (DTA). TGA/DTA was conducted using a Netzsch STA 409 PC thermal analyzer. Approximately 12 mg of potassium-jarosite/sodium-jarosite mineral was placed in a container of known mass. Samples were heated from 30 to 1000°C at 1 °C/min in flowing air (75 cm^3/min). The XRD patterns were obtained after heating potassium-jarosite and sodium-jarosite minerals, respectively, in air to various relevant temperatures that were selected from the TGA/DTA profiles.

3. Results

3.1 K-jarosite

The initial crystal structure of sample BY06-35 was confirmed by XRD, as shown in Fig. 1. The calculated unit cell parameters of BY06-35 are *a* = 7.326 Å and *c* = 16.619 Å. The SEM image in Fig. 2a shows that BY06-35 consists of euhedral tabular crystals 20–50 μm across. Based on EMP analysis, BY06-35 has an average composition of 6.73 wt% K_2O, 0.90 wt% Na_2O, 0.3 wt% PbO, 50.74 wt% Fe_2O_3, and 29.79 wt% SO_3, as shown in Table 2. The sample includes a minor amount of As_2O_3 substituted for S in the *X* site of the jarosite crystal structure. BY06-35 also contains a trace concentration of Al_2O_3 and P_2O_5.
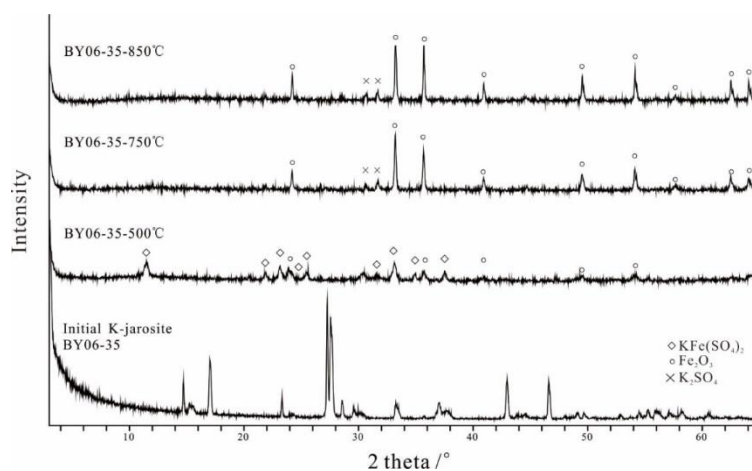
Fig. 1. X-ray diffraction patterns indicative of the thermal decomposition of potassium-jarosite (BY06-35) under atmospheric conditions
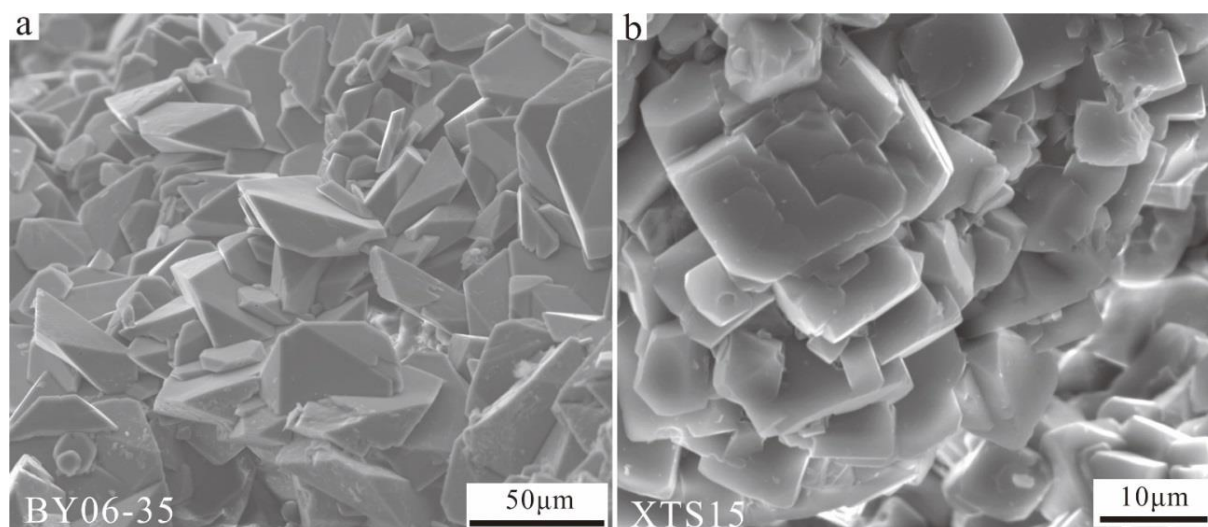
Fig. 2. Scanning electron microscopy images of potassium-jarosite (BY06-35) and sodium-jarosite (XTS15) crystals: (a) tabular morphologies of potassium-jarosite; (b) hexagonal pyramid morphologies of sodium-jarosite

The TGA/DTA profiles of sample BY06-35 is shown in Fig. 3a. The sample underwent a significant and abrupt mass loss during the heating process. The temperatures of the mass-loss events are assigned on the basis of peaks in the DTA curve. Sample BY06-35 released 11.39 wt% H_2O in a single event at ~443.0 °C, followed by a loss of 20.99 wt% SO_3 at 688.3 °C, and a final loss of 3.08 wt% at 779.3 °C (Fig. 3a). The XRD pattern of BY06-35 heated to 500°C shows the presence of $KFe(SO_4)_2$ and Fe_2O_3 (Fig. 1). As the temperature increased to 750 and 850 °C, the Fe_2O_3 provides sharper X-ray peaks, and the Fe_2O_3 and trace K_2SO_4 pattern remains at the highest temperature.
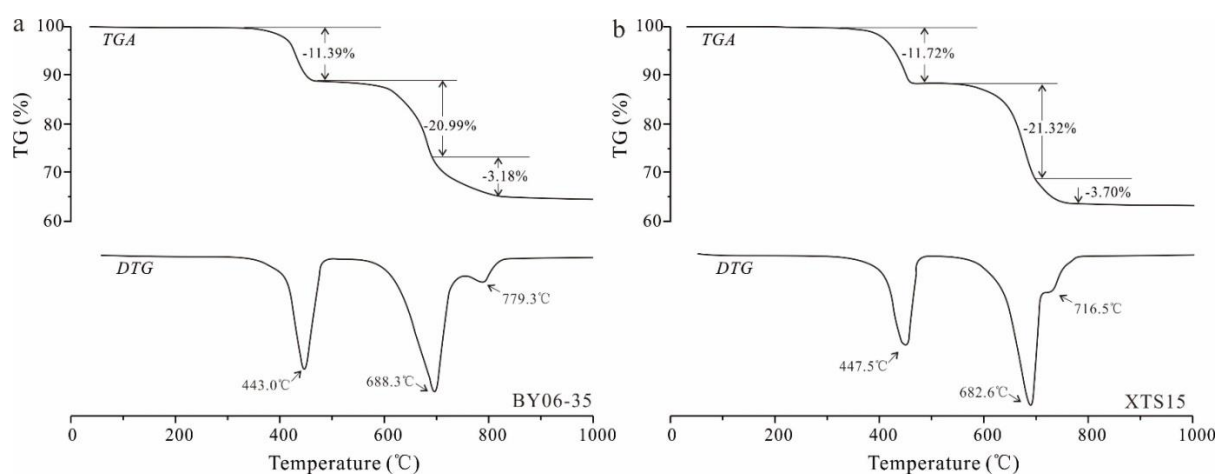
Fig. 3. Representative thermal analysis data of BY06-35 (potassium-jarosite; a) and XTS15 (sodium-jarosite; b). Thermogravimetric (TG) pattern shows the percentage mass loss relative to the initial sample mass as a function of temperature (°C). DTA is the first derivative of the TG signal

3.2 Na-jarosite

The initial crystal structure of sample XTS15 was confirmed by XRD, as shown in Fig. 4. The calculated unit cell parameters of XTS15 are a = 7.303 Å and c = 17.160 Å. The SEM image in Fig. 2b shows that XTS15 consists of hexagonal pyramid crystals that range from 5 to 10 μm. A comparison of the compositions of BY06-35 and XTS15 (Table 2) shows that XTS15 contains a lower amount of K_2O (0.20 wt%), but has a higher Na_2O concentration (5.90 wt%). The sample also contains 49.73 wt% Fe_2O_3, 32.84 wt% SO_3, minor amounts of P_2O_5 (0.07 wt%), and trace amounts of PbO and As_2O_3.

The TGA/DTA profiles of sample XTS15 is shown in Fig. 3b. Sample XTS15 released 11.72 wt% H_2O in a single event at ~447.5 °C, followed by a loss of 21.32 wt% SO_3 at 682.6 °C, and a final loss of

3.70 wt% at 716.5 °C (Fig. 3b). The XRD pattern of XTS15 heated to 500°C indicates that $NaFe(SO_4)_2$ is the major crystalline phase that is obtained at that temperature (Fig. 4). The XRD pattern of XTS15 heated to 700 and 800 °C shows only patterns that are indicative of Na_2SO_4 and Fe_2O_3.
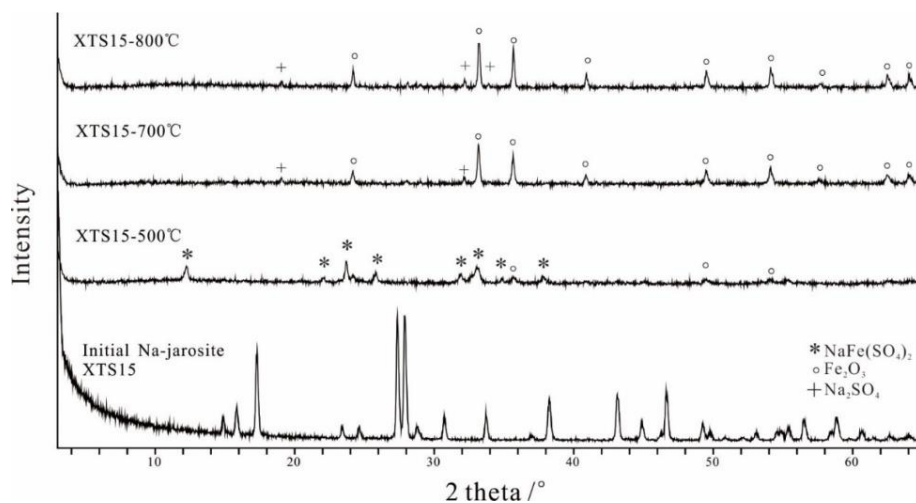
Fig. 4. X-ray diffraction patterns indicative of the thermal decomposition of sodium-jarosite (XTS15) under atmospheric conditions

Table 2. Chemical compositions (wt%) of natural supergene potassium jarosite (BY06-35) and sodium jarosite (XTS15) samples obtained by electron microprobe analysis. The components are based on the chemical formula $AB_3(XO_4)_2(OH)_6$
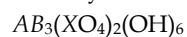
n	BY06-35 (4)	XTS15 (4)
K_2O	6.73	0.20
Na_2O	0.90	5.90
PbO	0.30	0.14
Fe_2O_3	50.74	49.73
Al_2O_3	0.03	0.01
SO_3	29.79	32.84
P_2O_5	0.04	0.07
As_2O_3	0.14	0.03
H_2O	11.75	11.08
Total	100.00	100.00
K	0.76	0.02
Na	0.16	0.92
Pb	0.01	0.00
Fe	3.40	3.03
Al	0.00	0.00
S	1.99	1.99
P	0.00	0.01
As	0.01	0.00
H	6.28	5.38
Total	12.61	11.35
ΣA	0.93	0.94
ΣB	3.40	3.03
ΣX	2.00	2.00

4. Discussion

4.1 Mechanism for decomposition of jarosite minerals

The thermal-decomposition mechanisms of potassium-jarosite and sodium-jarosite based on the analyses of samples BY06-35 and XTS15 are proposed as follows.

Jarosite step 1, dehydroxylation at 443.0 °C:

$$KFe_3(SO_4)_2(OH)_6 \rightarrow KFe(SO_4)_2 + Fe_2O_3 + 3H_2O.$$
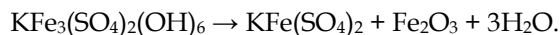
Based on the formula $KFe_3(SO_4)_2(OH)_6$, the theoretical mass loss because of dehydroxylation is 10.78%. The first large peak occurs at the point where the jarosite lattice is destroyed at 443.0 °C. The mass loss at this point is 11.39 wt%, which represents the loss of OH^-. The $KFe(SO_4)_2$ and Fe_2O_3 produced during decomposition is crystallized directly after a destruction of the jarosite lattice (Fig. 1).

Jarosite step 2, desulfonation at 688.3 and 779.3°C:

$$2KFe(SO_4)_2 \rightarrow K_2SO_4 + Fe_2O_3 + 3SO_3 \text{ (g)}.$$

The TGA/DTA curves show a large mass loss of 20.99 wt% at 688.3 °C. Little change in the crystal structure is observed above the second large peak, but sharper X-ray peaks that are representative of Fe_2O_3 indicate that crystal growth continues with increasing temperature. Presumably, the heating effect of the crystallization of Fe_2O_3, which occurs as a result of the decomposition of $KFe(SO_4)_2$ at 688.3 and 779.3 °C, is incorporated into the main peak.

The thermal behavior of sodium-jarosite is similar but is not strictly analogous to that of potassium-jarosite. The structures of the two minerals are essentially equivalent, and so, the chemical reactions upon heating are mostly the same.

Sodium-jarosite step 1, dehydroxylation at 447.5 °C:

$$NaFe_3(SO_4)_2(OH)_6 \rightarrow NaFe(SO_4)_2 + Fe_2O_3 + 3H_2O.$$

The mass loss at 447.5 °C is 11.72 wt%, which is similar to the theoretical mass loss (11.13%), and represents the loss of OH units from the sodium-jarosite structure.

Sodium-jarosite step 2, desulfonation at 682.6°C and 716.5°C:

$$2NaFe(SO_4)_2 \rightarrow Na_2SO_4 + Fe_2O_3 + 3SO_3 \text{ (g)}.$$

The TGA/DTA curves show a large mass loss of 21.32 wt% at 682.6 °C. XRD analyses of samples heated at 700 and 800 °C show the presence of hematite and Na_2SO_4 (Fig. 4). These results represent the complete thermal decomposition of $NaFe(SO_4)_2$.

4.2 Comparison of the thermal analyses of potassium-jarosite and sodium-jarosite

EMP analyses of samples BY06-35 and XTS15 demonstrated a limited substitution between K^+ and Na^+ in the potassium-jarosite and sodium-jarosite samples. Thus, the chemical formulas of potassium-jarosite and sodium-jarosite would be better written as $K_{0.76}Na_{0.16}Fe_{3.4}(SO_4)_{1.99}(As_2O_5)_{0.01}(OH)_{6.28}$ and $K_{0.02}Na_{0.92}Fe_{3.03}(SO_4)_{1.99}(P_2O_5)_{0.01}(OH)_{5.38}$, respectively. The atomic percentages of K in the potassium-jarosite and Na in the sodium-jarosite are less than those that are expected for the formula $K/NaFe_3(SO_4)_2(OH)_6$, which indicates a possible substitution for K^+ or Na^+ by H_3O^+ in the *A* site. However, the mass loss observed at 247°C for hydronium jarosite with the chemical formula as $K_{0.67}Na_{0.09}(H_3O)_{0.24}Fe_3(SO_4)_2(OH)_6$ (Alpers and Brimhall, 1989) was not observed in the TGA results for the potassium-jarosite and sodium-jarosite samples in this study (Figs 3a and b), which indicates an absence of H_3O^+ in the *A* site. The TGA/DTA results demonstrate that the thermal decomposition steps of potassium-jarosite occur at 443.0, 688.3, and 779.3°C. The TGA/DTA curves of potassium-jarosite in Fig. 3a are quite different from those reported in previous studies (Kulp and Adler, 1950; Drouet and Navrotsky, 2003; Frost et al., 2005). This is because of differences in the chemical composition between the supergene jarosite minerals and the synthetic jarosite samples. The Fe and K concentrations per unit formula of the synthesized jarosite samples used by Drouet and Navrotsky (2003) are less than theoretical values. Microprobe analyses showed that the iron and potassium components in the synthesized jarosites $((K_{0.86}H_3O_{0.14})Fe_{2.69}(SO_4)_2(OH_{5.07}H_2O_{0.93})$; Drouet and Navrotsky 2003) were less than 3 and 1, respectively. Nielsen et al. (2007) suggested that vacancies at

the *B* site could cause the formation of H_2O in the *A* site, which results in the release of H_2O molecules below 400°C from synthetic samples during TGA. The vacancies at the *B* site easily occur in the synthetic samples. Consequently, the TGA/DTA curves presented in other studies are more similar to the curves for hydronium jarosite decomposition obtained by Frost et al. (2006). This suggests that low Fe occupancy in the *B* site may alter the form of TGA/DTA curves to be more like that of hydronium jarosite. The EMP results show that the Fe concentrations per unit formula of samples BY06-35 and XTS15 are 3.40 and 3.03 (Table 2). Thus, there is no substitution of H_3O^+ in the *A* site of our samples and the consequent H_2O loss below 400°C in this study.

Thermal decomposition steps of sodium-jarosite were observed at 447.5, 682.6 and 716.5°C. The differences between the TGA/DTA curves obtained for the potassium-jarosite and sodium-jarosite samples could result from the K and Na contents, because the enthalpy of formation of potassium jarosite (-3829.6 kJ/mol, Drouet and Navrotsky, 2003) is lower than that of sodium jarosite (-3783.4 kJ/mol, Drouet and Navrotsky, 2003). Compared with potassium-jarosite, the initiation of lattice destruction occurs at a higher temperature for sodium-jarosite.

5. Conclusions

TGA/DTA coupled with XRD was used to investigate the thermal decomposition of supergene potassium-jarosite and sodium-jarosite mineral samples from northern China. The potassium-jarosite sample exhibited mass-loss events over a wide temperature range from 443.0 to 688.3°C and 779.3°C. The individual decomposition steps are represented by a loss of OH^- groups and SO_3. The primary solid intermediate products were $KFe(SO_4)_2$ and Fe_2O_3. The final solid products were Fe_2O_3 and K_2SO_4. For the sodium-jarosite sample, mass-loss events were observed at slightly different temperatures of 447.5, 682.6 and 716.5°C. The primary solid intermediate products were $NaFe(SO_4)_2$ and Fe_2O_3, and the final solid products were Fe_2O_3 and Na_2SO_4. A comparison of the thermal decomposition processes of supergene minerals with previously reported synthetic jarosite samples suggests that a low Fe occupancy may change the form of the TGA/DTA curves to be more like that of hydronium jarosite. A comparison of the thermal decomposition processes of potassium-jarosite and sodium-jarosite confirms that sodium-jarosite has a higher dehydroxylation temperature.

References

ALPERS, C. N., BRIMHALL, G. H., 1989. *Paleohydrologic evolution and geochemical dynamics of cumulative supergene metal enrichment at La Escondida, Atacama Desert, northern Chile*. Econ. Geol., 84, 229–255.

CHEN, L., 2012. *Mineralogy, geochemistry and $^{40}Ar/^{39}Ar$ geochronology of supergene minerals from typical sulfide deposits, NE Tibetan Plateau*. PhD thesis China University of Geosciences, Wuhan, 180.

CHEN, L., LI, J., 2014. $^{40}Ar/^{39}Ar$ *ages and stable isotopes of supergene jarosite from the Baiyin VHMS ore field, NE Tibetan Plateau with paleoclimatic implications*. Chinese Sci. Bull., 59, 2999-3009.

CHEN, L., LI, J., RYE, R. O., BENZEL, W. M., LOWERS, H. A., HE, M., 2013. *Mineralogical, chemical, and crystallographic properties of supergene jarosite-group minerals from the Xitieshan Pb-Zn sulfide deposit, northern Tibetan Plateau, China*. Miner. Petrol., 107, 487-499.

DESBOROUGH, G. A., SMITH, K. S., LOWERS, H. A., SWAYZE, G. A., HAMMARSTROM, J. M., DIEHL, S. F., LEINZ, R. W., DRISCOLL, R. L., 2010. *Mineralogical and chemical characteristics of some natural jarosites*. Geochim. Cosmochim. Ac., 74, 1041–1056.

DROUET, C., NAVROTSKY, A., 2003. *Synthesis, characterization, and thermochemistry of K-Na-H₃O jarosites*. Geochim. Cosmochim. Ac., 67, 2063–2076.

DUTRIZAC, J. E., JAMBOR, J. L., 2000. *Jarosites and their application in hydrometallurgy*. Rev. Mineral. Geochem., 40, 405–452.

FROST, R. L., WEIER, M. L., MARTENS, W., 2005. *Thermal decomposition of jarosites of potassium, sodium and lead*. J. Therm. Anal. Calorim., 82, 115–118.

FROST, R. L., WILLS, R. A., KLOPROGGE, J. T., MARTENS, W. N., 2006. *Thermal decomposition of hydronium jarosite (H₃O)Fe₃(SO₄)₂(OH)₆*. J. Therm. Anal. Calorim., 83, 213–218.

JAMBOR, J. L., 1999. *Nomenclature of the alunite supergroup*. Can. Mineral., 37, 1323–1341.

KUBISZ, J., 1971. *Studies on Synthetic alkali-hydronium jarosites. II. Thermal investigations*. Mineralogia Polonica, 2, 51–66.

KULP, J. L., ADLER, H. H., 1950. *Thermal study of jarosite*. Am. J. Sci., 248, 475–487.

NIELSEN, U. G., MAJZLAN, J., PHILLIPS, B., ZILIOX, M., GREY, C. P., 2007. *Characterization of defects and the local structure in natural and synthetic alunite (K, Na, H₃O)Al₃(SO₄)₂(OH)₆ by multi-nuclear solid-state NMR spectroscopy*. Am. Mineral., 92, 587–597.

RYE, R. O., ALPERS, C. N., 1997. *The stable isotope geochemistry of jarosite*. U.S. Geol. Surv. Open-File Rep., 88–97.

RYE, R. O., BETHKE, P. M., LANPHERE, M. A., STEVEN, T. A., 2000. *Neogene geomorphic and climatic evolution of the central San Juan Mountains, Colorado: K/Ar age and stable isotope data on supergene alunite and jarosite from the Creede mining district*. Geological Society of America Special Papers, 346, 95–103.

SCOTT, K. M., 1987. *Solid solution in, and classification of, gossan-derived members of the alunite-jarosite family, Northwest Queensland, Australia*. Am. Mineral., 72, 178–187.

STOFFREGEN, R. E., ALPERS, C. N., JAMBOR, J. L., 2000. *Alunite-Jarosite crystallography, thermodynamics, and geochronology*. Rev. Mineral. Geochem., 40, 453–479.